

Correlating Hemodynamic Magnetic Resonance Imaging with high-field Intracranial Vessel Wall Imaging in Stroke

Weston Langdon¹, Manus J. Donahue², Anja G. van der Kolk³, Swati Rane², Megan K. Strother^{4*}

1. Vanderbilt University School of Medicine, Nashville, USA

2. Vanderbilt University Institute of Imaging Science, Vanderbilt University Medical Center, Nashville, USA

3. Department of Radiology, University Medical Center Utrecht, Utrecht, The Netherlands

4. Department of Radiology and Radiological Sciences, Vanderbilt University Medical Center, Nashville, USA

* **Correspondence:** Megan K. Strother, Department of Radiology and Radiological Sciences, Vanderbilt University Medical Center, 1161 21st Avenue South, Nashville, TN 37232-2675, USA
(✉ Megan.strother@vanderbilt.edu)

Radiology Case. 2014 Jun; 8(6):1-10 :: DOI: 10.3941/jrcr.v8i6.1795

ABSTRACT

Vessel wall magnetic resonance imaging at ultra-high field (7 Tesla) can be used to visualize vascular lesions noninvasively and holds potential for improving stroke-risk assessment in patients with ischemic cerebrovascular disease. We present the first multi-modal comparison of such high-field vessel wall imaging with more conventional (i) 3 Tesla hemodynamic magnetic resonance imaging and (ii) digital subtraction angiography in a 69-year-old male with a left temporal ischemic infarct.

CASE REPORT

CASE REPORT

Clinical history

A 69-year-old male with past medical history significant for hypertension and hyperlipidemia reported being in his usual state of health at work when he became acutely confused and was unable to speak. He presented to the hospital with receptive and expressive aphasia and was able to follow only simple commands. Motor, sensory and cranial nerve exams were normal. Echocardiogram performed at admission was normal, leaving stroke etiology unclear. Therefore, we investigated the application of novel functional magnetic resonance imaging MRI approaches, such as vessel-encoded arterial spin labeling (VE-ASL) [1] and hypercarbic blood oxygen level dependent (BOLD) [2] imaging at 3T, to better understand perfusion traits. Furthermore, we employed high-resolution vessel wall imaging technique [3] at 7T to examine the presence of lesions and stenosis that may not have been apparent with conventional approaches.

Materials and Methods

Patient provided informed, written consent for the hemodynamic and vessel wall imaging studies and local

Institutional Review Board approval was obtained for the analyses.

Conventional Imaging: Non-contrasted axial CT (320mAs, 120 kV) and contrasted computed tomography angiography (CTA) (helical CTA, 200 mAs, 120 kV, 0.8 mm slice thickness, 150 mL Optiray 350 contrast) of the head were performed. Following CT, contrast-enhanced T1-weighted and diffusion-weighted MRI images were obtained using standard imaging protocols. Subsequently, three vessel digital subtraction angiography (DSA) was performed to characterize the mass encasing the left ICA and evaluate for intracranial arterial disease not seen on CTA.

Hemodynamic Imaging at 3T: We used novel functional MR imaging approaches including vessel-encoded arterial spin labeling (VE-ASL) and blood oxygen level dependent (BOLD) imaging at 3T to better understand perfusion. Patient provided informed, written consent for the hemodynamic and vessel wall imaging studies and local Institutional Review Board approval was obtained for the analyses. The hemodynamic 3T MR included:

(i) T1-weighted (MPRAGE: $1 \times 1 \times 1 \text{ mm}^3$; TR/TE=8.9/4.6 ms),

(ii) T2-weighted Fluid Attenuated Inversion Recovery (FLAIR) at a spatial resolution of $0.9 \times 0.9 \times 1 \text{ mm}^3$ at TR/TE=11000/120 ms,

(iii) VE-pCASL ($3.4 \times 3.4 \times 5 \text{ mm}^3$; TR/TE/TI=4000/17/1650 ms; 16 slices) to investigate perfusion territories of left internal carotid artery (ICA), right ICA, and the posterior circulation for tissue-level compromise and collateral compensation

(iv) Hypercarbic BOLD ($3.4 \times 3.4 \times 5 \text{ mm}^3$; TR/TE=2000/35 ms; 30 slices) using a block paradigm of 3/3 min baseline/5% carbogen (5% CO₂; 95% O₂) breathing repeated twice. Patient vitals (heart rate, blood pressure, pulse oximetric saturation and end-tidal CO₂: EtCO₂) were recorded throughout the scan. BOLD and VE-ASL MRI data were corrected for motion, baseline drift, and co-registered first to the anatomical T1-weighted images and then to standard MNI space [5]. For signal change detection and z-statistic classification, standard temporal autocorrelation routines incorporating a linear model and noise prewhitening were applied to BOLD data, which was pre-smoothed spatially using a Gaussian kernel with full-width-half-max (FWHM)=3 mm [6]. For BOLD analysis, voxel-by-voxel measurements were made for: (i) cerebral vascular reactivity (CVR), quantified as mean equilibrated signal in response to hypercarbia; and (ii) z-statistic with hypercarbia, indicative of the statistical strength of the BOLD response normalized by the noise. For VE-ASL, pair-wise subtraction of the label image from the control image was performed and the difference images were averaged. Subsequently, a single-compartment kinetic model incorporating the flow-modified solution to the Bloch equation was applied to quantify CBF using a constrained nonlinear optimization routine, in absolute units (ml/100g/min) on a voxel-by-voxel basis [7]. Flow territories were calculated upon application of a previously published k-means clustering algorithm [8,9]. Although hypercarbia is not a direct or natural measure of autoregulatory capacity, prior studies have demonstrated correlation between measurements of CVR with hypercarbic stimulus and disease severity [10, 11].

Imaging at 7T: Following 3T hemodynamic MRI and DSA, high spatial resolution ($0.8 \times 0.8 \times 0.8 \text{ mm}^3$) T1-weighted magnetization prepared inversion recovery turbo spin-echo sequence (MPIR-TSE) was used for intracranial arterial wall imaging [12]. In this method, cerebrospinal fluid (CSF) signal is nulled using an adiabatic inversion pre-pulse (analogous to FLAIR MRI) and flowing blood is dephased due to incomplete refocusing during the turbo spin echo readout. Vessels surrounded by relatively larger volumes of CSF, such as the Circle of Willis, are most clearly imaged with this approach.

Findings

Non-contrast CT (Fig. 1a) and contrast-enhanced CTA (Fig. 1b) of the head showed vasogenic edema in the inferior left frontal lobe with a partially calcified left planum ethmoidalis and paraclinoid mass (2.1cm x 1.0cm x 3.3cm)

and hyperostosis, which was confirmed by MRI (Fig. 1c). Diffusion weighted MRI also showed scattered areas of restricted diffusion, which is confirmed by apparent diffusion coefficient maps, secondary to acute infarction in the left middle cerebral artery (MCA) territory cortex (Fig. 2). Contrast-enhanced T1-weighted MRI images (Fig. 3) demonstrated a homogeneously enhancing mass encasing the left ICA and extending into the suprasellar cistern. Imaging characteristics were highly suggestive of meningioma [4].

Hypercarbic BOLD revealed compromised CVR (Fig. 4c) within the left MCA territory subacute stroke. VE-ASL imaging showed apparent increase in CBF in the subacute stroke, which could be due to "luxury perfusion" or endovascular signal due to delayed arterial transit times (Fig. 5).

DSA (Fig. 6) confirmed the hypervascular appearance of the suspected meningioma. DSA also showed focal stenosis in the left distal anterior cerebral artery (ACA), MCA and posterior cerebral artery (PCA) branches (Fig. 7). The portion of the left ICA surrounded by the mass and the right ICA were not affected. On 7T MRI arterial wall imaging, three non-stenosing arterial plaques affecting the A1 segment of the left ACA, the proximal M1 segment of the left MCA and the posterior wall of the basilar artery were revealed which were not visualized on DSA (Fig. 7d-f).

Management

Secondary stroke prevention begun after discharge from the hospital included antiplatelet therapy (aspirin 81mg daily). Anti-hypertensive and anti-hyperlipidemia medications were continued, with a target systolic blood pressure < 130 mm Hg and low-density lipoprotein (LDL) < 100 mg/dL.

Follow up

Six months following initial stroke, cardiac Holter monitoring revealed paroxysmal atrial fibrillation secondary to sick sinus syndrome and patient underwent pacemaker implantation.

DISCUSSION

Etiology & demographics

Stroke is the third leading cause of death in the United States and the second most common cause of disability, affecting 795,000 people yearly [13]. Although two-thirds of stroke patients survive their stroke, half of these stroke survivors are left disabled [14]. For 2008, the estimated cost of stroke-related morbidity in the United States was \$65.5 billion [13]. The disease has a higher incidence in males than females at younger ages but the gender difference diminishes with advancing age. The majority of strokes are ischemic (87%) with hemorrhagic strokes comprising the other 13%. There are numerous modifiable risk factors for stroke, including hypertension, which increases the risk of stroke at age 50 four-fold; atrial fibrillation also increases stroke risk by a factor of four [15]. Persistent, paroxysmal, and permanent atrial fibrillation all appear to increase the risk of ischemic stroke to a similar degree [16].

Clinical & imaging findings

In this case, since luminal stenosis on DSA was only found within the left ICA territory, an embolic or stenosing effect from the suspected meningioma was considered. Large vessel embolic strokes affect the territory supplied by the affected artery, whereas infarcts due to systemic hypoperfusion typically cause bilateral findings except in the presence of lateralizing vascular stenosis. Cardioembolic strokes may affect more than one vascular territory. Angiographic support for ICA wall invasion by meningioma includes focal stenosis in the portion of the meningioma surrounded by the ICA, which was not found [17]. Histologic ICA invasion has been reported-despite a normal appearance of the ICA lumen on angiography-when a meningioma completely surrounds the ICA lumen, but the mass did not encompass the ICA in this patient [18]. Despite their infiltrative nature, meningiomas have rarely been associated with cerebral ischemia [19]. One review of all surgically evaluated meningioma patients found the incidence of meningioma-related cerebral ischemia to be 0.19% (three of 1617 meningiomas) [20]. Endovascular stenting and angioplasty of symptomatic ICA stenosis related to skull-based meningiomas have been reported [21,22]. Most published cases of cerebral ischemia secondary to meningioma are in the setting of severe ICA stenosis or occlusion [22,23]. Convexity and parasagittal meningiomas have been suggested to cause transient ischemic attacks by some authors [24,25]. However, identification of additional non-lumen compromising vessel wall lesions with 7T MRI, which included posterior circulation disease, suggested more generalized atherosclerotic disease rather than isolated left ICA embolic or stenosing changes arising from the presumed meningioma.

Hemodynamic imaging performed two months after the acute stroke showed hyperperfusion on arterial spin-labeling (ASL) MRI with decreased CVR on BOLD. In a prospective study using single photon emission computerized tomography (SPECT) to evaluate reperfusion in acute and subacute stroke, Bowler, et al., reported visually apparent reperfusion in 28% of patients (14 of 50), with a mean delay of 5.8 days. The authors found reperfusion was significantly more common in embolic strokes than strokes from other etiologies-with 13 of 23 embolic events reperfused but only 3 of 23 other events [26]. In this patient, increased CBF in the subacute stroke region may be hyperperfusion, luxury perfusion or artifact due to endovascular signal from delayed arterial transit times. Luxury perfusion implies excessive CBF compared to metabolic demand, which is typically measured with positron emission tomography (PET) [27].

This case demonstrates an application of innovative advanced diagnostic tools, including 7T-vessel wall and hemodynamic 3T MRI techniques, to characterize subacute stroke. With high-field vessel wall imaging, atherosclerotic plaques in the left ACA, left MCA and basilar artery were visualized despite normal findings on DSA. In this case, we used a 7T protocol which was optimized to show the Circle of Willis and adjacent arteries. However, recent reports demonstrate protocols for whole-brain intracranial vessel wall imaging which may allow for visualization of plaques in

smaller vessels [28]. Eventually, plaques may be able to be further characterized for high-risk features.

7T intracranial vessel wall imaging is limited currently by strict safety guidelines not applied to imaging at lower magnetic fields. Additionally, inhomogeneity of the transmit-field at 7T makes imaging of the temporal and occipital lobe vessel walls difficult. However, prior studies using intracranial vessel wall imaging have shown promising results in detecting non-stenosing atherosclerotic plaques and other intracranial arterial wall pathology, like vasculitis. As non-invasive MR methods are prospectively evaluated in clinical trials, these techniques, which can be performed in less than one hour without intravenous contrast or radiation, may contribute to a better understanding of the etiology of stroke and the tissue-level hemodynamics which underlie its clinical manifestations.

Treatment & prognosis

Hemodynamic MRI and DSA confirmed a lack of flow failure in the left ICA related to the paraclinoid mass. DSA has been the gold standard for evaluating neurovascular compromise, but is invasive and requires exogenous contrast. In contrast, noninvasive measurement of hemodynamic impairment with MRI is readily accessible for most treatment centers, due to technical innovations over the past decade, and can be performed and processed within an hour. Without evidence for flow failure, vessel wall imaging was performed to assess for thrombotic etiology, but lesions found in the anterior and posterior circulation were non-stenosing. The relative risk from flow failure due to luminal stenosis compared to ruptured atherosclerotic plaque intracranially is unknown. Much more is known about coronary and carotid bifurcation risk factors. For instance, nearly 70% of acute coronary events are caused by lesions that are not hemodynamically significant or flow limiting prior to the event [29]. Carotid bifurcation studies have identified "vulnerable" plaque features which increase stroke risk [30], including lipid-rich necrotic cores [31], intra-plaque hemorrhage [32-34] and torn fibrous caps [35]. Improved understanding of the longitudinal progression of atherosclerosis has shown that early extra-cranial carotid bifurcation plaque is accommodated by external remodeling without luminal compromise [36], presumably in an attempt to preserve hemodynamic flow. However, differences in the hemodynamic forces, lumen and wall thickness, shear stress, and wall motion within intracranial vessels could lead to varying manifestations and significance of intracranial plaque compared to extracranial atherosclerosis. Intracranial wall imaging has only recently become technically feasible, and thus longitudinal studies are necessary to understand the clinical implications for the non-stenosing wall lesions identified in this patient.

Six months after the patient's initial stroke, telemetry revealed paroxysmal atrial fibrillation secondary to sick sinus syndrome. Given the strong cardioembolic source, stroke etiology was felt to be embolic, rather than related to the intracranial vessel wall lesions or the presumed meningioma. Patient was then anticoagulated with warfarin and a permanent pacemaker was implanted. Pacemaker placement may reduce morbidity, but has not been shown to reduce mortality, in patients with sick sinus syndrome [37].

Differential Diagnoses for stroke etiology:

The Trial of Org 10172 in Acute Stroke Treatment (TOAST) classification system is the most widely utilized for stroke subtype classification [38]. The five subtypes are 1) large-artery atherosclerosis, 2) cardioembolism, 3) small-vessel occlusion, 4) stroke of other determined etiology, and 5) stroke of undetermined etiology. Clinical presentation can often help determine the etiology of stroke. For instance, this patient presented with aphasia, which is a cortical sign. Other cortical signs include agnosia, neglect, apraxia, or hemianopsia. Patients presenting with cortical signs more often are suffering from embolic stroke. In contrast, small-vessel occlusions typically cause lacunar infarcts in the territory of penetrating basal arteries and are not typically associated with cortical findings. The most common clinical presentations for lacunar infarcts include pure motor hemiparesis, pure sensory stroke, and ataxic hemiparesis [39]. In this case, after large-artery atherosclerosis was excluded, the abrupt onset of maximum symptoms favored an embolic etiology, which was confirmed with the identification of sick sinus syndrome. Over half of patients with sick sinus syndrome have alternating bradycardia and atrial tachyarrhythmia, even with pacing, with atrial fibrillation the most common [40]. Within the TOAST classification, atrial fibrillation is a high-risk source for cerebrovascular events, which has been confirmed by subsequent studies [41]. Other high-risk sources include rheumatic mitral or aortic valve disease, recent myocardial infarction and recent coronary artery bypass graft surgery. Tse, et al., found episodes of atrial fibrillation occurred in 44% of patients with sick sinus syndrome (mean follow up 16 months), and was associated with a 2.5-fold increase in major cardiovascular events, especially stroke [42]. The risk of stroke in patients with atrial fibrillation should be determined and anticoagulation is indicated for patients at high risk for stroke [43].

TEACHING POINT

High field MRI using a vessel wall sequence may identify atherosclerotic plaques which are not well characterized by conventional imaging modalities such as DSA or CTA. Such information complements the hemodynamic evaluation of stroke which is obtained using advanced functional MRI.

REFERENCES

1. Wong EC. Vessel-encoded arterial spin-labeling using pseudocontinuous tagging. *Magn Reson Med.* 2007 Dec;58(6):1086-91. PMID: 17969084
2. Donahue MJ, Strother MK, Hendrikse J. Novel MRI approaches for assessing cerebral hemodynamics in ischemic cerebrovascular disease. *Stroke.* 2012 Mar;43(3):903-15. PMID: 22343644
3. van der Kolk AG, Zwanenburg JJ, Brundel M, et al. Intracranial vessel wall imaging at 7.0-T MRI. *Stroke.* 2011 Sep;42(9):2478-84. PMID: 21757674

4. Lee KF. The Diagnostic Value of Hyperostosis in Midline Subfrontal Meningioma - An Analysis of 66 Cases. *Radiology.* 1976 Apr;119(1):121-130. PMID: 943801
5. Jenkinson M, Smith S. A global optimization method for robust affine registration of brain images. *Med Image Anal.* 2001;5(2):143-56. PMID: 11516708
6. Woolrich MW, Ripley BD, Brady M, Smith SM. Temporal autocorrelation in univariate linear modeling of FMRI data. *Neuroimage.* 2001;14(6):1370-86. PMID: 11707093
7. Buxton RB, Frank LR, Wong EC, Siewert B, Warach S, Edelman RR. A general kinetic model for quantitative perfusion imaging with arterial spin labeling. *Magn Reson Med.* 1998;40(3):383-96. PMID: 9727941
8. Gevers S, Bokkers RP, Hendrikse J, et al. Robustness and reproducibility of flow territories defined by planning-free vessel-encoded pseudocontinuous arterial spin-labeling. *Am J Neuroradiol.* 2012 Feb;33(2):E21-5. PMID: 21393410
9. Donahue MJ, Hussey E, Rane S, et al. Vessel-encoded arterial spin labeling (VE-ASL) reveals elevated flow territory asymmetry in older adults with substandard verbal memory performance. *J Magn Reson Imaging.* 2014 Feb;39(2):377-86. PMID: 23633160
10. Heyn C, Poublanc J, Crawley A, et al. Quantification of cerebrovascular reactivity by blood oxygen level-dependent MR imaging and correlation with conventional angiography in patients with Moyamoya disease. *Am J Neuroradiol* 2010;31:862-867. PMID: 20075092
11. Donahue MJ, Ayad M, Moore R, et al. Relationships between hypercarbic reactivity, cerebral blood flow, and arterial circulation times in patients with moyamoya disease. *J Magn Reson Imaging.* 2013 Nov;38(5):1129-39. PMID: 23440909
12. van der Kolk AG, Hendrikse J, Brundel M, et al. Multi-sequence whole-brain intracranial vessel wall imaging at 7.0 tesla. *Eur Radiol.* 2013 Nov;23(11):2996-3004. PMID: 23736375
13. Rosamond W, Flegal K, Furie K. et al. Heart Disease and Stroke Statistics 2008 Update. A Report From the American Heart Association Statistics Committee and Stroke Statistics Subcommittee. *Circulation.* 2008;117(4):e25-e146. PMID: 18086926
14. Anderson CS, Linto J, Stewart-Wynne EG. A population-based assessment of the impact and burden of caregiving for long-term stroke survivors. *Stroke.* 1995;26:843-9. PMID: 7740578
15. Goldstein LB, Adams R, Alberts MJ, et al. Primary Prevention of Ischemic Stroke: A Guideline From the American Heart Association/American Stroke Association Stroke Council. *Stroke.* 2006;37:1583-633. PMID: 16675728
16. Hart RG, Pearce LA, Rothbart RM, McAnulty JH, Asinger RW, Halperin JL. Stroke With Intermittent Atrial Fibrillation: Incidence and Predictors During Aspirin Therapy. *J Am Coll Cardiol.* 2000 Jan;35(1):183-7. PMID: 10636278
17. Ishikawa M, Nishi S, Aoki T, et al. Predictability of internal carotid artery (ICA) dissectability in cases showing ICA involvement in parasellar meningioma. *J Clin Neurosci.* 2001 May;8 Suppl 1:22-5. PMID: 11386821
18. Sen C, Hague K. Meningiomas involving the cavernous sinus: histological factors affecting the degree of

- resection. *J Neurosurg.* 1997 Oct;87(4):535-43. PMID: 9322844
19. Abdel-Aziz KM, Froelich SC, Dagnew E, et al. Large sphenoid wing meningiomas involving the cavernous sinus: conservative surgical strategies for better functional outcomes. *Neurosurgery.* 2004 Jun;54(6):1375-83; discussion 1383-4. PMID: 15157294
 20. Komotar RJ, Keswani SC, Wityk RJ. Meningioma presenting as stroke: report of two cases and estimation of incidence. *J Neurol Neurosurg Psychiatry.* 2003 Jan;74(1):136-7. PMID: 12486289
 21. Heye S, Maleux G, Van Loon J, Wilms G. Symptomatic stenosis of the cavernous portion of the internal carotid artery due to an irresectable medial sphenoid wing meningioma: treatment by endovascular stent placement. *Am J Neuroradiol.* 2006 Aug;27(7):1532-4. PMID: 16908574
 22. Chivoret N, Fontaine D, Lachaud S, Chau Y, Sedat J. Endovascular angioplasty before resection of a sphenoidal meningioma with vascular encasement. *Interv Neuroradiol.* 2011 Sep;17(3):391-4. PMID: 22005706
 23. Mourad A, Guichard JP, Vignal C, Boussier MG, Vahedi K. Sphenoid and optic nerve sheath meningioma revealed by recurrent brain infarctions. *Rev Neurol (Paris).* 2009 Dec;165(12):1092-4. PMID: 19324384
 24. Cameron EW. Transient ischaemic attacks due to meningioma--report of 4 cases. *Clin Radiol.* 1994 Jun;49(6):416-8. PMID: 8045068
 25. Kaur U, Chopra JS, Kak VK, Banerjee AK. Meningioma presenting as recurrent transient cerebral ischemia and intracranial hemorrhage. *Surg Neurol.* 1982 Feb;17(2):120-2. PMID: 7200265
 26. Bowler JV, Wade JP, Jones BE, Nijran KS, Steiner TJ. Natural history of the spontaneous reperfusion of human cerebral infarcts as assessed by 99mTc HMPAO SPECT. *J Neurol Neurosurg Psychiatry.* 1998 Jan;64(1):90-7. PMID: 9436735
 27. Oku N, Kashiwagi T, Hatazawa J. Nuclear neuroimaging in acute and subacute ischemic stroke. *Ann Nucl Med.* 2010 Nov;24(9):629-38. PMID: 20953742
 28. van der Kolk AG, Hendrikse J, Brundel M, et al. Multi-sequence whole-brain intracranial vessel wall imaging at 7.0 tesla. *European Radiology.* 2013 Nov;23(11):2996-3004. PMID: 23736375
 29. Falk E, Shah PK, Fuster V. Coronary plaque disruption. *Circulation.* 1995 Aug 1;92:657-71. PMID: 7634481
 30. van Gils MJ, Vukadinovic D, van Dijk AC, Dippel DWJ, Niessen WJ, van der Lugt A. Carotid Atherosclerotic Plaque Progression and Change in Plaque Composition Over Time: A 5-Year Follow-Up Study Using Serial CT Angiography. *Am J Neuroradiol.* 2012;33:1267-73. PMID: 22345501
 31. Kwee RM, van Oostenbrugge RJ, Mess WH, et al. MRI of Carotid Atherosclerosis to Identify TIA and Stroke Patients Who Are at Risk of a Recurrence. *J Magn Reson Imaging.* 2013 May;37(5):1189-94. PMID: 23166040
 32. Altaf N, MacSweeney ST, Gladman J, et al. Carotid intraplaque hemorrhage predicts recurrent symptoms in patients with high-grade carotid stenosis. *Stroke.* 2007;38:1633-35. PMID: 17379827
 33. Altaf N, Daniels L, Morgan PS, et al. Detection of intraplaque hemorrhage by magnetic resonance imaging in symptomatic patients with mild to moderate carotid stenosis predicts recurrent neurological events. *J Vasc Surg.* 2008; 47:337-42. PMID: 18164171
 34. Kurosaki Y, Yoshida K, Endo H, et al. Association between carotid atherosclerosis plaque with high signal intensity on T1-weighted imaging and subsequent ipsilateral ischemic events. *Neurosurgery.* 2011;68:62- 67, discussion 67. PMID: 21099723
 35. Redgrave JN, Gallagher P, Lovett JK, Rothwell PM. Critical Cap Thickness and Rupture in Symptomatic Carotid Plaques. The Oxford Plaque Study. *Stroke.* 2008 Jun; 39(6):1722-9. PMID: 18403733
 36. Glagov S, Weisenberg E, Zarins CK, Stankunavicius R, Kolettis GJ. Compensatory Enlargement of Human Atherosclerotic Coronary Arteries. *N Engl J Med.* 1987 May 28;316(22):1371-5. PMID: 3574413
 37. Cheng A. Manifestations and causes of the sick sinus syndrome. Wolters Kluwer Health. UpToDate.com. Nov 2012. Available at: <http://www.uptodate.com/contents/manifestations-and-causes-of-the-sick-sinus-syndrome?selectedTitle=1~150>
 38. Adams HP Jr, Bendixen BH, Kappelle LJ, et al. Classification of subtype of acute ischemic stroke. Definitions for use in a multicenter clinical trial. TOAST. Trial of Org 10172 in Acute Stroke Treatment. *Stroke.* 1993 Jan;24(1):35-41. PMID: 7678184
 39. Caplan LR. Clinical diagnosis of stroke subtypes. Wolters Kluwer Health. UpToDate.com. Dec 2012. Available at: <http://www.uptodate.com/contents/clinical-diagnosis-of-stroke-subtypes?selectedTitle=1~150>.
 40. Lamas GA, Lee KL, Sweeney MO, et al. Ventricular pacing or dual-chamber pacing for sinus-node dysfunction. *N Engl J Med.* 2002 Jun 13;346(24):1854-62. PMID: 12063369
 41. Ay H, Furie KL, Singhal A, Smith WS, Sorensen AG, Koroshetz WJ. An evidence-based causative classification system for acute ischemic stroke. *Ann Neurol.* 2005 Nov;58(5):688-97. PMID: 16240340
 42. Tse HF, Lau CP. Prevalence and clinical implications of atrial fibrillation episodes detected by pacemaker in patients with sick sinus syndrome. *Heart.* 2005 91:362-364. PMID: 15710720
 43. Roger VL, Go AS, Lloyd-Jones DM, et al. on behalf of the American Heart Association Statistics Committee and Stroke Statistics Subcommittee. Heart disease and stroke statistics--2012 update: a report from the American Heart Association. *Circulation.* 2012 Jan 3;125(1):e2-e220. Erratum in *Circulation.* 2012 Jun 5;125(22):e1002. PMID: 22179539
 44. Doufekias E, Segal AZ, Kizer JR. Cardiogenic and aortogenic brain embolism. *J Am Coll Cardiol* 2008; 51:1049. PMID: 18342221
 45. Momjian-Mayor I, Baron JC. The pathophysiology of watershed infarction in internal carotid artery disease: review of cerebral perfusion studies. *Stroke.* 2005 Mar;36(3):567-77. PMID: 15692123
 46. Gottesman RF, Sherman PM, Grega MA, et al. Watershed strokes after cardiac surgery: diagnosis, etiology, and outcome. *Stroke.* 2006 Sep;37(9):2306-11. PMID: 16857947

FIGURES

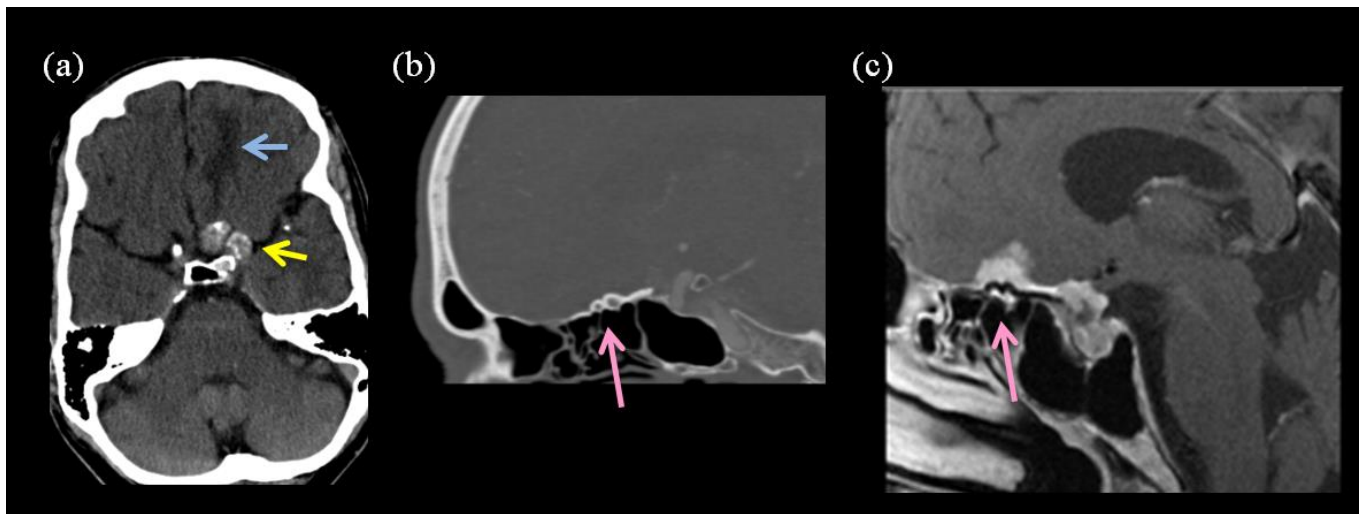


Figure 1: 69 year old male with meningioma.

FINDINGS: Axial non-contrast CT (a) shows calcified left paracallosal mass (yellow arrow) and vasogenic edema (blue arrow). Sagittal images from contrasted CTA (b) and T1-weighted MR (c) show hyperostosis of the planum ethmoidale (pink arrows) abutting the dural-based enhancing extra-axial mass which extends into the suprasellar cistern, an appearance characteristic of a meningioma.

TECHNIQUE: Axial CT, 320mAs, 120 kV; Helical CTA, 200 mAs, 120 kV, 0.8 mm slice thickness, 150 mL Optiray 350 contrast; Sagittal 1.5T T1-weighted MR (TR/TE=565/17 ms), 15 mL Magnevist contrast.

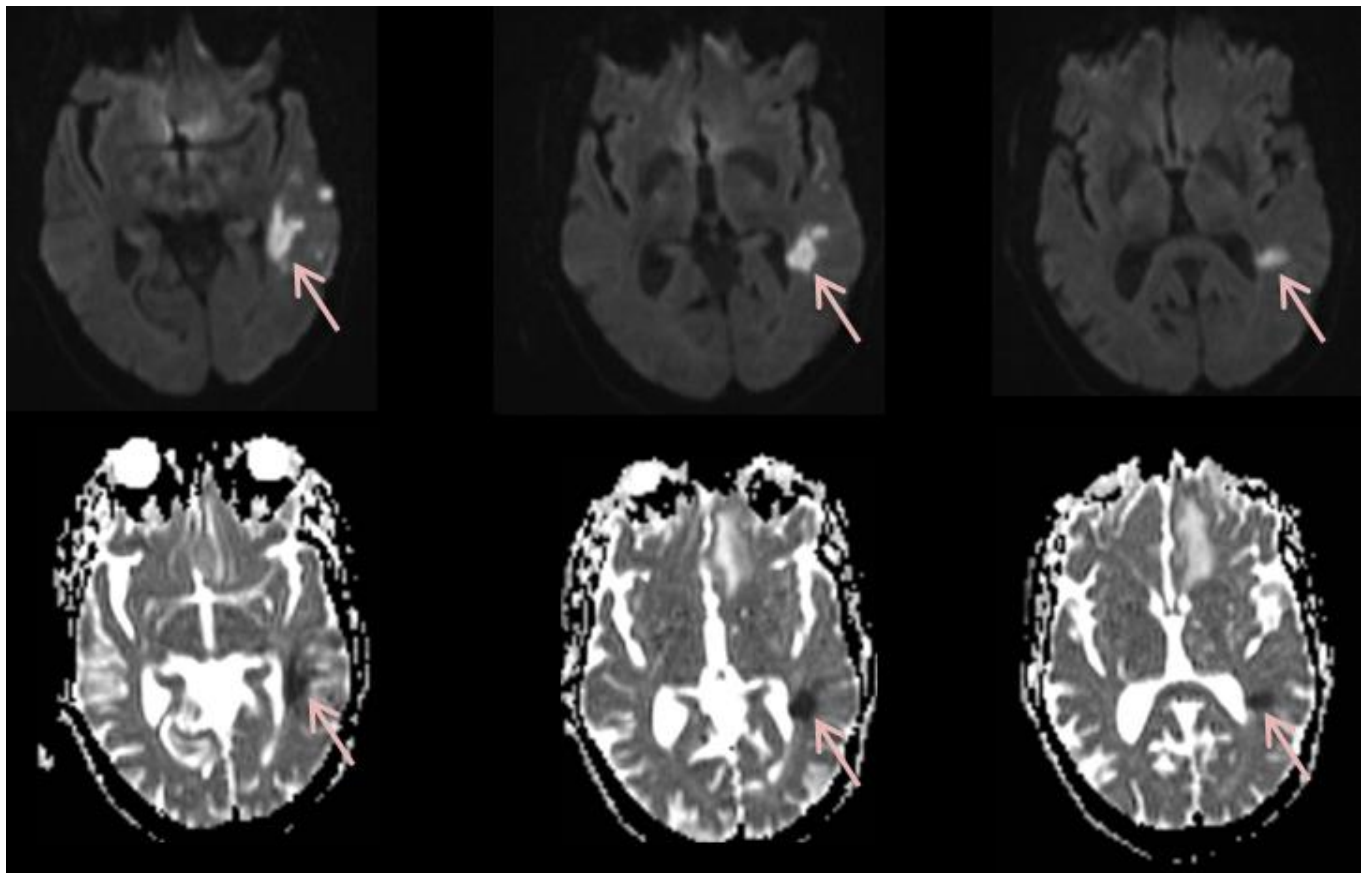


Figure 2: 69 year old male with acute infarct.

FINDINGS: Axial diffusion weighted images (DWI) (top) with corresponding axial apparent diffusion coefficient maps (ADC) (bottom) show scattered areas of restricted diffusion in left MCA territory (pink arrows).

TECHNIQUE: Axial 3T DWI MR (TR/TE =5600/118 ms).

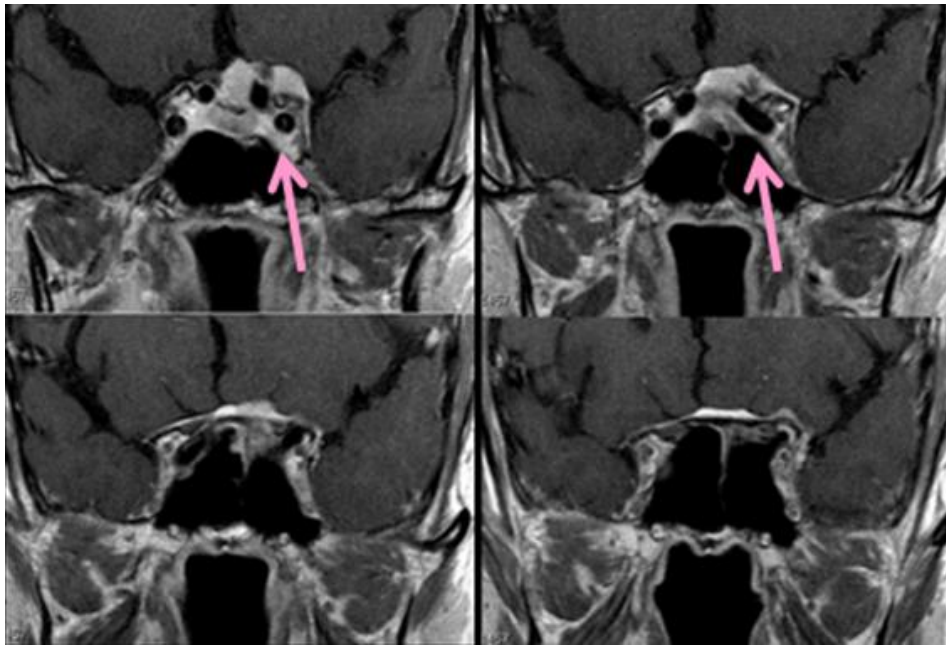


Figure 3: 69 year old male with meningioma.

FINDINGS: Coronal T1-weighted contrasted MR shows homogeneously enhancing suprasellar mass occupying the suprasellar cistern with dural tail, which abuts the left ICA. Note the left ICA lumen does not appear narrowed (pink arrows).

TECHNIQUE: Coronal 3T T1-weighted MR (TR/TE=750/9 ms), 15 mL Magnevist contrast.

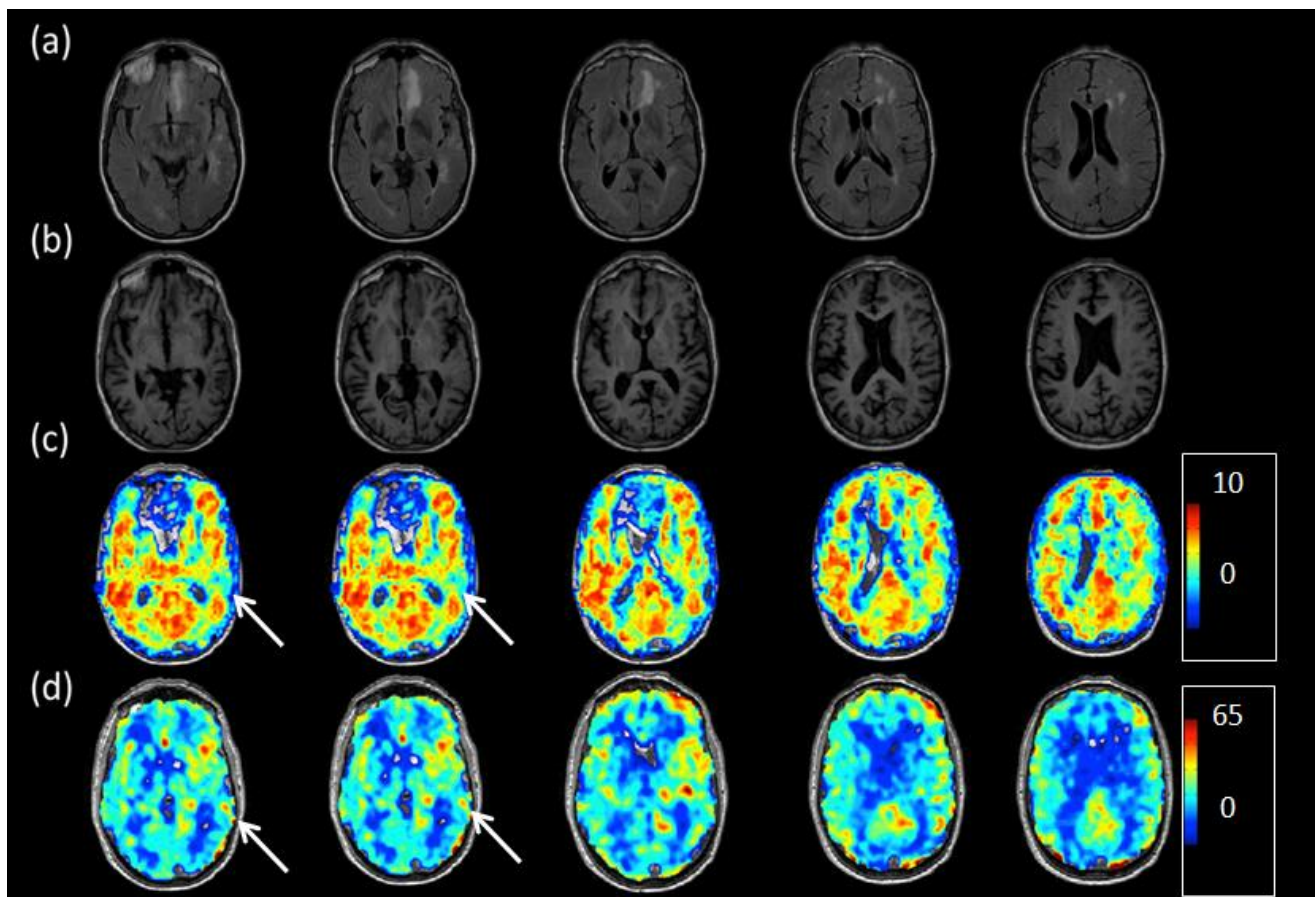


Figure 4: 69 year old male with subacute L MCA infarct. **FINDINGS:** Co-registered axial FLAIR (a), T1 (b), BOLD z-statistic (c), and ASL (d) images show decreased left MCA-territory CVR on BOLD and increased apparent CBF (mL/100g/min) on ASL (white arrows). This could be "luxury perfusion" or endovascular signal due to delayed transit times. **TECHNIQUE:** Axial 3T T2-weighted FLAIR (0.9x0.9x1 mm³; TR/TE=11000/120 ms); axial 3T T1-weighted (MPRAGE: 1x1x1 mm³; TR/TE=8.9/4.6 ms); axial 3T hypercarbic BOLD (3.4x3.4x5 mm³; TR/TE=2000/35 ms; 30 slices) using a block paradigm of 3/3 min baseline/5% carbogen (5% CO₂; 95% O₂) breathing repeated twice; axial 3T cerebral blood flow (CBF)-weighted pseudo-continuous ASL (3.4x3.4x5 mm³; TR/TE/TI=4000/17/1650 ms; 16 slices; bipolar dephasing gradients).

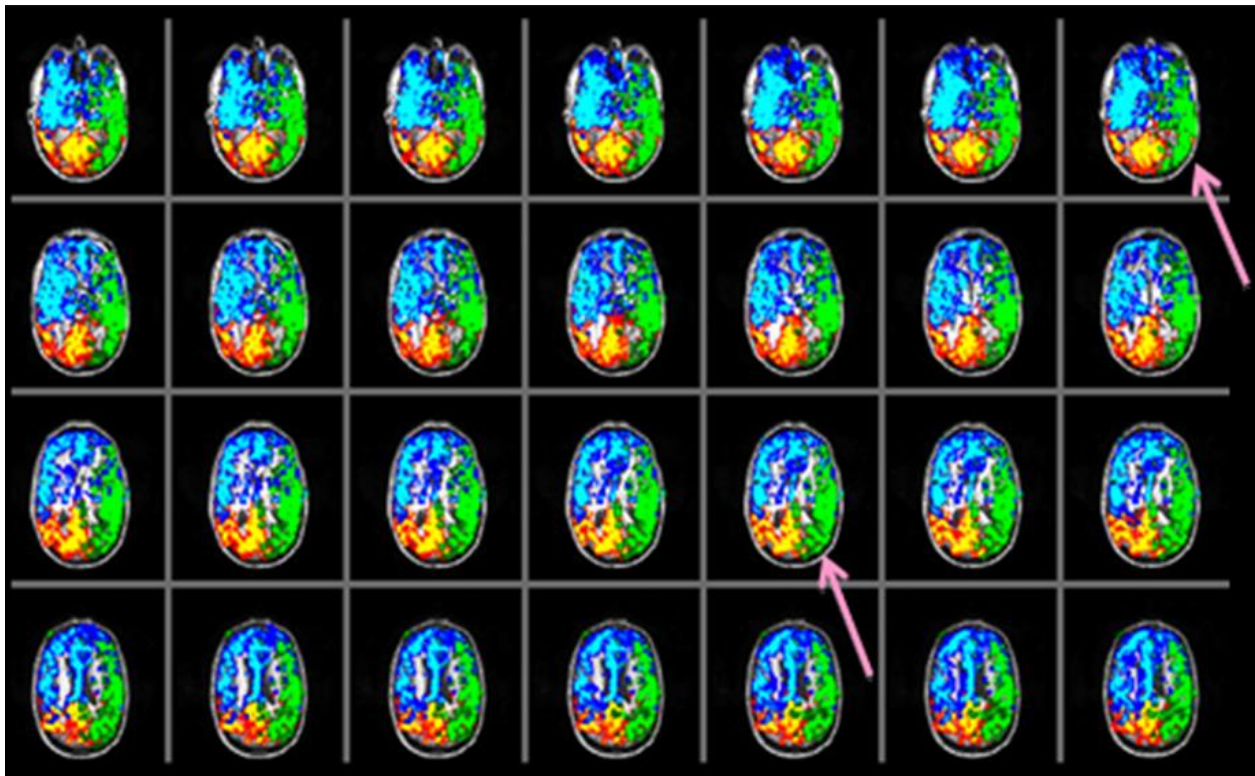


Figure 5: 69 year old male with subacute infarct.

FINDINGS: VE-ASL demonstrates the perfusion territories for the right ICA (blue), left ICA (green) and basilar tag (yellow). The fetal configuration PCOM is indicated by the left ICA perfusion to the left PCA territory (pink arrows).

TECHNIQUE: Axial 3T CBF-weighted VE-ASL (3.4x3.4x5 mm³; 16 slices; bipolar dephasing gradients, TR/TE/TI=4000/17/1650 ms;).

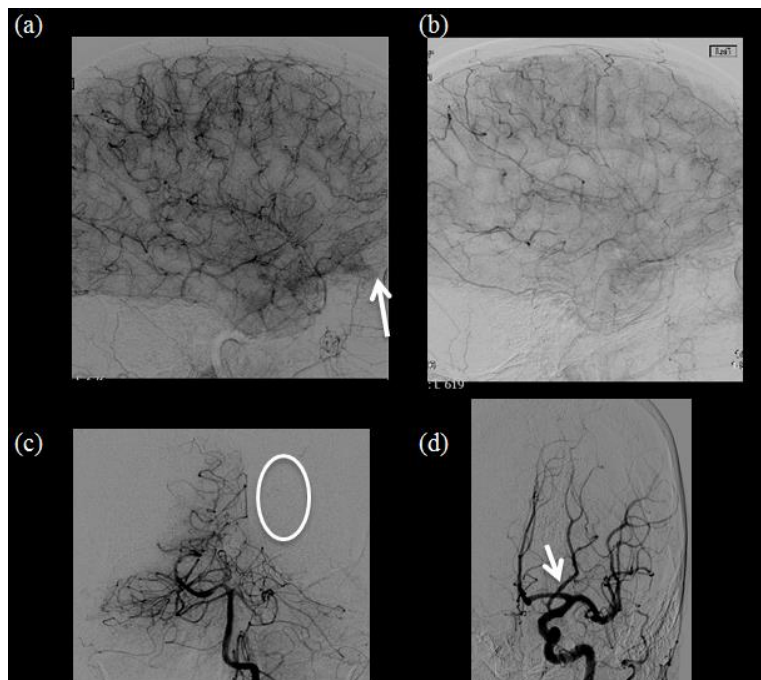


Figure 6: 69 year old male with mass and subacute infarct.

FINDINGS: Lateral projections on DSA from right (a) and left (b) CCA injections show hypervascular blush (white arrow) along the planum ethmoidalis meningioma from the right common carotid artery (CCA) injection. AP projection from left vertebral injection (c) shows lack of left occipital lobe perfusion (white circle). This territory is perfused from fetal PCOM (white arrow), opacified from CCA injection (d).

TECHNIQUE: DSA projections following right CCA (6mL Omnipaque 240 contrast/1 second), left vertebral artery and left CCA injections (4mL/s and 6mL/s Omnipaque 240 contrast).

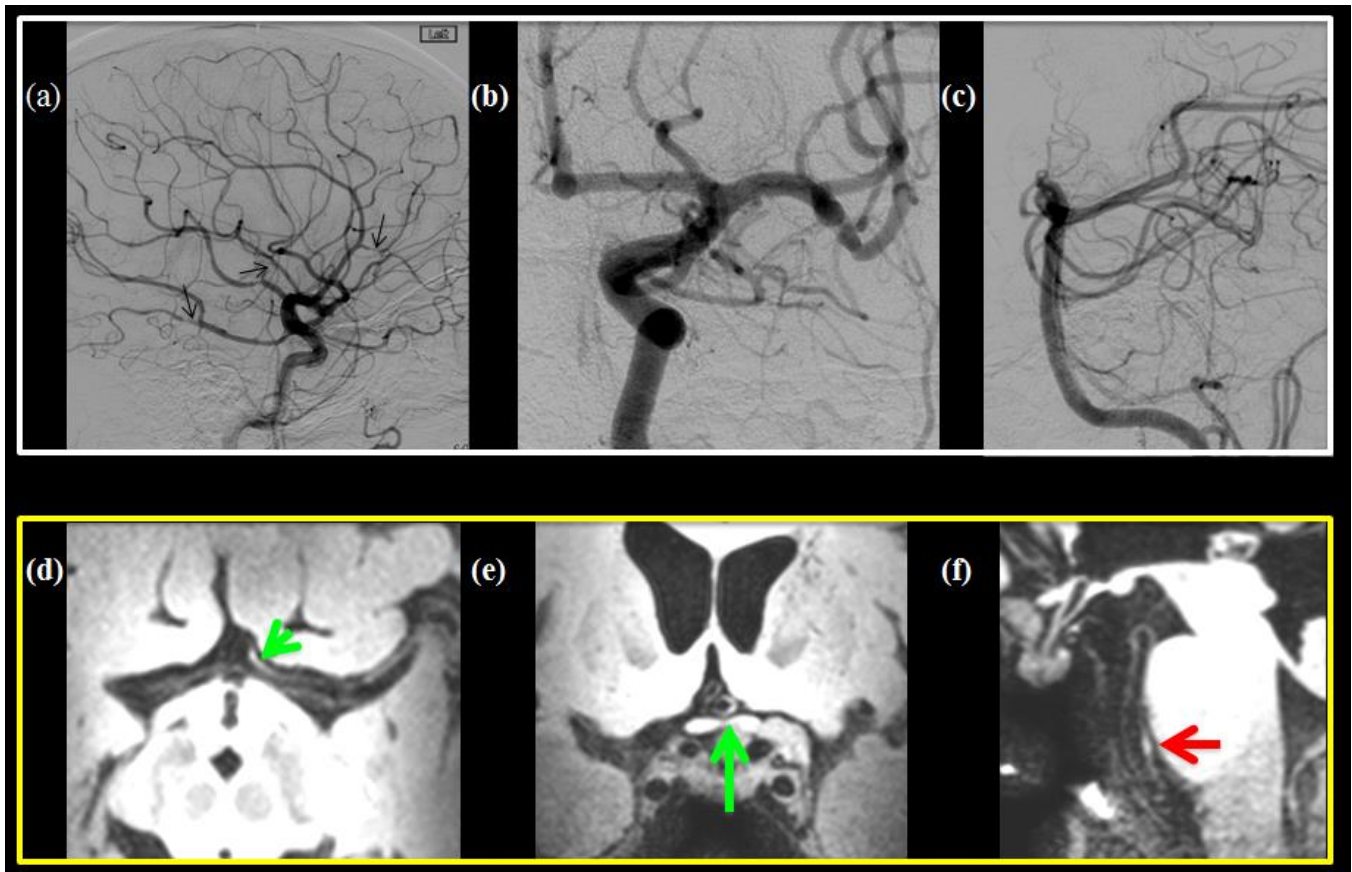


Figure 7: 69 year old male with subacute infarct.

FINDINGS: Lateral projection from left CCA injection (a) demonstrates scattered peripheral areas of luminal narrowing (black arrows). AP projection from left CCA injection (b) and lateral projection from left vertebral injection (c) show normal appearing A1 segment and basilar artery. However, 7T vessel wall imaging (axial "d", coronal "e", and sagittal "f") identifies non-stenosing plaques, which are not seen by lumenography (green arrows identify A1 lesions, red arrow identifies basilar lesion).

TECHNIQUE: DSA with vertebral and left CCA injections at 4mL/s and 6mL/s Omnipaque 240 contrast. With 7T MR (TR=3952 ms; 0.8 mm isotropic; 3D turbo spin echo TE=39 ms; duration= 7min), both CSF and blood water are nulled to reveal vessel wall and plaque contrast. A FLAIR inversion recovery pre-pulse nulls the longitudinal component of the CSF magnetization, whereby the turbo-spin-echo readout works to dephase the transverse magnetization of flowing blood water.

| | |
|--|--|
| Etiologies | <ul style="list-style-type: none"> • Ischemic (87%) • Hemorrhagic (13%) |
| Incidence [43] | <ul style="list-style-type: none"> • 795,000 strokes/year in the United States • Men>women at younger ages but not older |
| High-risk Cardioembolic Sources [41-44] | <ul style="list-style-type: none"> • Persistent, paroxysmal, and permanent atrial fibrillation all appear to increase the risk of ischemic stroke to a similar degree • Patients with atrial fibrillation have a 4-fold increased risk of ischemic stroke |
| Clinical course | <ul style="list-style-type: none"> • Embolic strokes most often occur suddenly, with maximum symptoms at onset • Thrombosis-related stroke symptoms may fluctuate |
| Treatment | <ul style="list-style-type: none"> • Chronic anticoagulation is recommended for patients with atrial fibrillation if the patient is determined to be at high risk for stroke and no contraindications are present. |
| Findings on Imaging | <ul style="list-style-type: none"> • Cardioembolic strokes may affect more than one vascular territory • Ischemic strokes may occur in a watershed distribution [45] • Systemic hypoperfusion may cause bilateral findings, but can be unilateral in the setting of asymmetric neurovascular disease [46] |

Table 1: Summary table for stroke subtypes [43]

| Anterior Circulation Stroke Subtype | Infarct Location | Clinical Presentation | Tests |
|-------------------------------------|------------------------------------|---|-------------------------|
| Cardioembolism | Cortical or subcortical | Cortical dysfunction (e.g. aphasia, agnosia, neglect, apraxia, or hemianopsia) | Abnormal Echocardiogram |
| Large-artery atherosclerosis | Cortical or subcortical | Cortical dysfunction | ICA or MCA stenosis |
| Small-artery occlusion | Basal penetrating artery territory | Lacunar syndrome (e.g. pure motor hemiparesis, pure sensory stroke, and ataxic hemiparesis) | Infarct < 20 mm |

Table 2: Differential table for stroke subtypes

The etiologic classification of stroke subtype is made by combining criteria from clinical presentation with outcomes from diagnostic tests.

ABBREVIATIONS

- ACA = Anterior cerebral artery
- ASL = Arterial spin-labeling
- BOLD = Blood oxygenation level-dependent
- CBF = Cerebral blood flow
- CSF = Cerebral spinal fluid
- CT = Computed tomography
- CVR = Cerebral vascular reactivity
- DSA = Digital subtraction angiography
- ICA = Internal carotid artery
- MCA = Middle cerebral artery
- MRI = Magnetic resonance imaging
- PCA = Posterior cerebral artery
- pCASL = Pseudocontinuous arterial spin-labeling
- PET = Positron emission tomography
- SPECT = Single photon emission computerized tomography
- TOAST = Trial of Org 10172 in Acute Stroke Treatment
- VE-ASL = Vessel encoded arterial spin-labeling

KEYWORDS

Stroke; Cerebral Stroke; Cerebrovascular Accident; Cerebrovascular Stroke; Meningioma; Intracranial Meningioma; vessel-wall imaging; fMRI; Magnetic Resonance Imaging, Functional; MRI, Functional; Atherosclerosis

Online access

This publication is online available at:
www.radiologycases.com/index.php/radiologycases/article/view/1795

Peer discussion

Discuss this manuscript in our protected discussion forum at:
www.radiolopolis.com/forums/JRCR

Interactivity

This publication is available as an interactive article with scroll, window/level, magnify and more features.
 Available online at www.RadiologyCases.com

Published by EduRad



www.EduRad.org